Chemistry and Physics of Lipids 229 (2020) 104892

Contents lists available at ScienceDirect

Chemistry and Physics of Lipids

journal homepage: www.elsevier.com/locate/chemphyslip

The structures of polyunsaturated lipid bilayers by joint refinement of neutron and X-ray scattering data

Drew Marquardt[a,b,*], Frederick A. Heberle[c], Jianjun Pan[d], Xiaolin Cheng[e], Georg Pabst[f], Thad A. Harroun[g], Norbert Kučerka[h], John Katsaras[g,i,j,k,l,*]

[a] Department of Chemistry and Biochemistry, University of Windsor, Windsor, ON, Canada
[b] Department of Physics, University of Windsor, Windsor, ON, Canada
[c] Department of Chemistry, University of Tennessee, Knoxville, TN 37996, USA
[d] Department of Physics, University of South Florida, Tampa, FL USA
[e] Division of Medicinal Chemistry and Pharmacognosy, The Ohio State University, Columbus, OH, USA
[f] University of Graz, Institute of Molecular Biosciences, Biophysics Division, 8010 Graz, Austria
[g] Department of Physics, Brock University, St. Catharines, ON, Canada
[h] Joint Institute for Nuclear Research, Frank Laboratory of Neutron Physics, Dubna, Russia and Department of Physical Chemistry of Drugs, Faculty of Pharmacy, Comenius University in Bratislava, Slovakia
[i] The Bredesen Center, University of Tennessee, Knoxville, TN, USA
[j] Shull Wollan Center, Oak Ridge National Laboratory, Oak Ridge, TN, USA
[k] Large Scale Structures Group, Neutron Sciences Directorate, Oak Ridge National Laboratory, Oak Ridge, TN, USA
[l] Department of Physics and Astronomy, University of Tennessee, Knoxville, TN, USA

ARTICLE INFO

Keywords:
Polyunsaturated fatty acids
Neutron scattering
X-ray scattering
MD simulations

ABSTRACT

We present the detailed structural analysis of polyunsaturated fatty acid-containing phospholipids namely, 1-palmitoyl-2-docosahexaenoyl-*sn*-glycero-3-phosphocholine (PDPC) and 1-stearoyl-2-docosahexaenoyl-*sn*-glycero-3-phosphocholine (SDPC). A newly developed molecular dynamics (MD) simulation parsing scheme for lipids containing fatty acids with multiple double bonds was implemented into the scattering density profile (SDP) model to simultaneously refine differently contrasted neutron and X-ray scattering data. SDP analyses of scattering data at 30 °C yielded lipid areas of 71.1 Å^2 and 70.4 Å^2 for PDPC and SDPC bilayers, respectively, and a model free analysis of PDPC at 30 °C resulted in a lipid area of 72 Å^2. In addition to bilayer structural parameters, using area-constrained MD simulations we determined the area compressibility modulus, K_A, to be 246.4 mN/m, a value similar to other neutral phospholipids.

1. Introduction

Phospholipids that contain polyunsaturated fatty acids (PUFAs) are a special class of lipids that constitute a biologically influential group of biomolecules essential for normal growth and development (O'Connor et al., 2001). Recently, PUFA-containing phospholipids have attracted increased attention as they have been shown to be essential for a range of cellular functions (Hamilton et al., 2000) and for their structural and functional roles in membranes (Catalá, 2012). PUFAs are generally classified as *omega*-3 or *omega*-6 fatty acids, depending on the location of the double bond in relation to the acyl chain's terminal methyl group (i.e., *omega*-3 has its last double bond located three atoms from the terminal methyl group). The dietary consumption of *omega*-3 fatty acids is known to alleviate chronic health conditions including, hypertension, diabetes, and arthritis (Stillwell and Wassall, 2003; Simopoulos, 2000), while a diet rich in *omega*-6 fatty acids is linked to increased blood viscosity, vasospasm, and vasoconstriction (Simopoulos, 1999). However, there is increasing evidence that both PUFAs (i.e., *omega*-3 and *omega*-6) are needed for maintaining good health (Simopoulos, 2004) and an imbalance results in diseases such as, diabetes (Simopoulos, 2000).

PUFAs associated with phospholipids also exhibit increased dynamics compared to their saturated analogues. For example, the low energy barrier for rotation about C-C single bonds between olefanic and aliphatic carbons in PUFAs allows for sub-nanosecond conformational transitions, resulting in a much higher degree of chain disorder, which

* Corresponding authors at: Department of Chemistry and Biochemistry, University of Windsor, Windsor, ON, Canada; Large Scale Structures Group, Oak Ridge National Laboratory, Oak Ridge, TN, United States.
E-mail addresses: drew.marquardt@uwindsor.ca (D. Marquardt), katsarasj@ornl.gov (J. Katsaras).

https://doi.org/10.1016/j.chemphyslip.2020.104892
Received 15 November 2019; Received in revised form 18 January 2020; Accepted 10 February 2020
Available online 12 February 2020
0009-3084/

increases the interaction probability between PUFAs and the lipid headgroups (Eldho et al., 2003). In the case of docosahexaenoic acid (DHA; 22:6) containing lipids, it has been shown that DHA explores its entire conformational space in ~50 ns (Soubias and Gawrisch, 2007). The high degree of PUFA chain disorder also results in thinner bilayers. An example is diarachidonoyl PC (DAPC; di20:4PC), which has an acyl chain thickness comparable to 1,2-dilauroyl-sn-glycero-3-phosphocholine (DLPC; di12:0PC), even though DAPC has eight more methines per hydrocarbon chain (Marquardt et al., 2013; Harroun et al., 2006). However, a more telling example of PUFA chain disorder is given by their segmental order parameters (S_{CD}). Both simulation (Leng et al., 2015) and experimental results (Feller et al., 2002; Gawrisch et al., 2003) show reduced S_{CD} values (S_{CD} <0.05) along the length of DHA chains in SDPC bilayers as a result of increased mobility associated with their double bonds. Moreover, mixed chain PUFA PCs, such as 1-palmitoyl-2-arachidonoyl-sn-glycero-3-phosphocholine (PAPC; 16:0-20:4PC) and 1-stearoyl-2-docosahexaenoyl-sn-glycero-3-phosphocholine (SDPC; 18:0-22:6PC), have been reported to form thinner bilayers with larger areas per lipid, compared to bilayers whose lipids contain either a saturated or mono-unsaturated fatty acid chain in their *sn*-2 position. In addition to their high mobility, PUFAs are susceptible to reactive oxygen species. Their vulnerability to oxidation creates unique biological problems, both structurally and in terms of biological availability. Structurally, PUFA oxidation products can alter the physical properties of a bilayer, which can ultimately lead to the malfunction of membrane associated proteins.

Although not common, PUFA-containing phospholipid simulations do exist. However, it appears that in some cases, the existing force fields result in physically unrealistic bilayer values. For example, Klauda et al. reported a headgroup-headgroup spacing (D_{HH}) for DAPC (Klauda et al., 2012) that is similar to the D_{HH} of POPC (36 Å), (Kučerka et al., 2011) but much larger than the experimentally determined value (Marquardt et al., 2013; Harroun et al., 2008). Inconsistencies between experiment and simulations thus pose significant problems when trying to accurately explain the physical behavior of PUFA containing phospholipids.

Here, we present a scattering density profile (SDP) model for lipids with PUFAs, namely the mixed chain lipids 1-palmitoyl-2-docosahexaenoyl-*sn*-glycero-3-phosphocholine (PDPC; 16:0-22:6PC) and 1-stearoyl-2-docosahexaenoyl-*sn*-glycero-3-phosphocholine (SDPC; 18:0-22:6PC). Combining small angle X-ray scattering (SAXS), small angle neutron scattering (SANS), and molecular dynamics (MD) simulations, we determined their bilayer structures with a high degree of accuracy and unprecedented spatial resolution.

2. Materials and methods

2.1. Materials

Synthetic 1-palmitoyl-2-docosahexaenoyl-*sn*-glycero-3-phosphocholine (PDPC) and 1-stearoyl-2-docosahexaenoyl-*sn*-glycero-3-phosphocholine (SDPC) were purchased from Avanti Polar (Alabaster, AL) lipids as chloroform solutions and used as received. Ultrapure H_2O was obtained from a High-Q purification system (Wilmette, IL), and 99.9% D_2O was purchased from Cambridge Isotopes (Andover, MA).

2.2. Vesicle preparation

Large unilamellar vesicles (LUVs) were prepared using previously established procedures (Kučerka et al., 2011; Heberle et al., 2013). In short, PDPC films were prepared by transferring the desired volumes of stock lipid solutions to glass vials (Hamilton USA, Reno, NV) and then evaporating the organic solvent using a combination of Ar gas and gentle heating, followed by drying in vacuo for no less than 4 h. Samples were then hydrated with 100% D_2O for SANS measurements, or ultrapure H_2O for SAXS measurements, using a series of 7 freeze-thaw-vortex cycles. The lipid dispersions were extruded using an Avanti mini-extruder with a 50 nm diameter pore size polycarbonate filter. The SANS sample was then divided into three aliquots and diluted to the desired external contrast condition (i.e., 100, 75, and 50% D_2O) using an appropriate amount of H_2O. The lipid concentration used for SAXS and SANS measurements was ~12 mg/ml. To minimize lipid oxidation, all sample manipulations were performed in a Techni-Dome 360° Glove Box Chamber under an Ar atmosphere. Oxygen was measured with an Oxy-Sen oxygen monitor (Alpha Omega Instruments, Cumberland, RI) and maintained below 2% for all sample manipulations. Aliquots of the PUFA samples were taken before and after SANS measurements to evaluate oxidative damage as determined by UV/Vis spectroscopy. UV/vis experiments were conducted with an Ocean Optics USB4000 CCD array detector coupled to an RF deuterium source with a tungsten halogen bulb (Mississauga, Canada) using the procedure described by Marquardt et al. (2013).

2.3. Density measurements

Lipid dispersions for volume measurements were prepared by hydrating ~25 mg of PDPC or SDPC with ~1.5 g of degassed ultrapure H_2O, followed by gentle sonication at room temperature until the dispersion was uniformly "milky" in appearance. Care was taken to avoid exposure of the sample to oxygen, thus sample manipulations were carried out in an Ar atmosphere (O_2 < 2%). The temperature dependent densities of water (ρ_w) and of the lipid dispersions (ρ_s) were determined by a temperature-controlled Anton-Paar DMA5000 (Graz, Austria) vibrating tube densitometer. The lipid volume (V_L), at a given temperature, was calculated as previously described (Kratky et al., 1973; Hodzic et al., 2008; Pan et al., 2012)

$$V_L = \frac{MW_L}{N_A \rho_s}\left[1 + \frac{m_w}{m_s}\left(1 - \frac{\rho_s}{\rho_w}\right)\right] \quad (1)$$

where MW_L is the molecular weight of the lipid, N_A is Avogadro's number, and m_L and m_W are the masses of the lipid and water, respectively.

2.4. Small-angle neutron and X-ray scattering

X-ray data were taken at the Cornell High Energy Synchrotron Source (CHESS) G-1 station. 1.18 Åwavelength X-ray photons were detected using a 1024 × 1024 pixel array FLICAM charge-coupled device (CCD) with 71 μm linear dimension pixels. Samples were taken up in 1 mm quartz capillaries placed in a homemade temperature-controlled, multiple position sample holder. Neutron scattering experiments were performed at the High Flux Isotope Reactor (HFIR) CG-3 Bio-SANS instrument located at Oak Ridge National Laboratory (ORNL). ULV suspensions were loaded into 2 mm path-length quartz banjo cells (Hellma USA, Plainview, NY), sealed under an Ar atmosphere, and mounted in a temperature-controlled cell holder. Data were taken at a sample-to-detector distance (SDD) of 1.7 m using 6 Åwavelength neutrons ($\Delta\lambda/\lambda = 0.15$), resulting in a total scattering vector of $0.02 < q < 0.3$ Å^{-1}. Scattered neutrons were collected using a 192 × 192 pixel two-dimensional (1 m × 1 m) ^{3}He position-sensitive detector (ORDELA, Inc., Oak Ridge, TN). Two-dimensional data were reduced into a one-dimensional scattering intensity (I) vs. the scattering vector (q) plot using ORNL's MANTID software (Arnold et al., 2014).

2.5. Molecular dynamics simulations

The CHARMM-GUI Membrane Builder (Jo et al., 2009) was used to generate coordinates for a PDPC bilayer containing a total of 200 lipids. Lipid hydrogen atoms were explicit (all-atom model), including 6962 water molecules. MD simulations were performed using the NAMD 2.9 (Phillips et al., 2005) and CHARMM 36 lipid force fields (Klauda et al.,

2010). Periodic boundary conditions were applied and for each system, energy was minimized using the conjugated gradient algorithm for 5000 steps, followed by 2 ns of equilibration in a constant particle number, pressure, and temperature (NPT) ensemble. Equilibrium was determined by monitoring the system's area per lipid and its root-mean-square deviation (RMSD). In all simulations, the van der Waals (vdW) interactions were truncated via a potential-based switching function used in X-PLOR. Starting from a switching distance of 8 Å, the vdW force was brought smoothly to zero at the cut-off distance of 12 Å. Electrostatic interactions were treated using the particle-mesh Ewald (PME) method with a 1.0 Å grid spacing (Darden et al., 1993). The r-RESPA multiple-time-step method (Tuckerman et al., 1992) was used with a 2 fs time step for bonded, and 2 and 4 fs time steps for short-range nonbonded and long-range electrostatic interactions, respectively. Bonds between hydrogens and other atoms were constrained using the SHAKE algorithm (Ryckaert et al., 1977).

We first simulated the PDPC bilayer using the NPT ensemble for 80 ns. Langevin dynamics were used to maintain a constant temperature of 303 K, while the Nose-Hoover Langevin-piston algorithm (Martyna et al., 1992; Feller et al., 1995) was used to maintain a constant pressure of 1 bar. The z-axis was allowed to expand and contract independently of the x-y plane (semi-isotropic pressure coupling). The resulting equilibrated lipid area was 63.5 Å^2. This simulation was then used to guide the development of an SDP model for the joint analysis of the SAXS and SANS data that resulted in an area per lipid of 70.2 Å^2. An additional set of 7 constant particle number, area, normal pressure, and temperature (NAPnT) simulations was performed, where the average area per lipid was constrained to 64, 66, 68, 70, 72, 74, and 76 Å^2, while the z-axis was allowed to expand and contract in order to maintain a constant pressure. Starting configurations for these simulations were selected snapshots from the NPT trajectory with lipid areas set close to their target values. The production run length for each of these simulations was between 96 and 128 ns, of which only the final 50 ns of each trajectory were used for data analysis. For each of the area-constrained simulations, the surface tension, γ, was calculated from the difference between the normal and lateral components of the pressure tensor (Sonne et al., 2005; Berger et al., 1997). The lateral area compressibility modulus, K_A, was given by $K_A = \partial\gamma/\partial(\ln A)$ (Braun et al., 2013). All simulations were conducted on the Hopper supercomputer located at the National Energy Research Scientific Computing Center (NERSC).

3. Results and discussion

3.1. Sample integrity

As noted, PUFA's are extremely sensitive to oxidative damage. Thus, to determine if any oxidative damage occurred over the course of a given measurement, we performed UV/vis measurements. The majority of naturally occurring carbon-based free radicals are formed from the alkyl and allylic carbons in the lipid acyl chains. Allylic carbon radicals quickly isomerize, conjugating the double bonds in PUFAs, and resulting in the electron-π system that absorbs UV light. After SANS experimentation, small amounts of oxidized lipids were detected as a small increase in absorbance around 250 nm (Fig. 1, red curve), compared to a fresh lipid preparation (Fig. 1, blue curve). However, when comparing samples that underwent experimentation to those exposed intentionally to air (Fig. 1, yellow and red curves, respectively), the amount of oxidative damage incurred by the SANS samples was negligible. Moreover, successive frames of SAXS data did not show any signs of sample degradation.

3.2. Insight from area constrained MD simulations

Simulations were performed using lipid areas ranging from 64.0 to 76.0 Å^2, generating a series of neutron and X-ray form factors for each

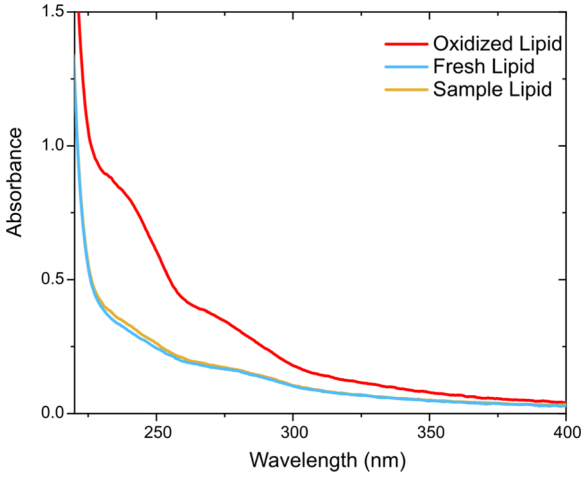

Fig. 1. UV absorption spectra of SDPC bilayers composed of oxidized lipid (red line), freshly prepared lipid (blue), and a sealed sample studied by SANS approximately 12 h after the measurement (orange line). The oxidized lipid was exposed to air for 12 h.

system. Bilayer form factors were generated by computing the number density distribution of each atom from the simulation trajectories (Kučerka et al., 2010). Electron density and neutron scattering length density profiles were calculated by summing the product of the number density of each atom with its number of electrons or neutron scattering length, respectively. The corresponding simulated X-ray and neutron scattering form factors were calculated, respectively, from the Fourier transform of the solvent-subtracted ED or NSLD profile, as was done previously (Klauda et al., 2010; Pan et al.. 2014a,b; Kučerka et al., 2015). The quality of the model-free analysis compares the calculated form factors with those from experiment, where the agreement between the two was quantified by a reduced χ^2 defined as:

$$\chi^2 = \frac{1}{N_q - 1}\sum_{i=1}^{N}\left(\frac{|F_s(q_i)| - k \times |F_e(q_i)|}{k \times \Delta F_e(q_i)}\right)^2, \quad (2)$$

where N_q is the number of experimental q-values (data points), F_s and F_e are the simulated and experimental form factors, respectively, ΔF_e is the experimental uncertainty, and k is a scaling factor used to minimize χ^2.

Fig. 2 displays the reduced neutron, X-ray, and overall χ^2 as a function of simulated area per lipid for PDPC at 30 °C measured at three different SANS contrasts (i.e., 100, 75 and 50% D_2O) and one SAXS

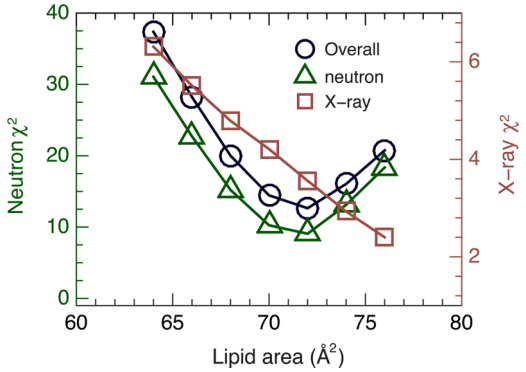

Fig. 2. Model-free comparisons between experimental and simulated form factors for predetermined PDPC lipid areas. The neutron χ^2 (open triangle, left axis) were obtained by summing the squares of the neutron form factor differences at 3 D_2O contrasts (i.e., 100, 75 and 50% D_2O) and weighted by their experimental uncertainties and number of data points. The X-ray χ^2 (open square, right axis) were obtained in a similar manner, except that there was only one set of X-ray data. The overall χ^2 (open circle, left axis) was obtained from a combination of neutron and X-ray χ^2.

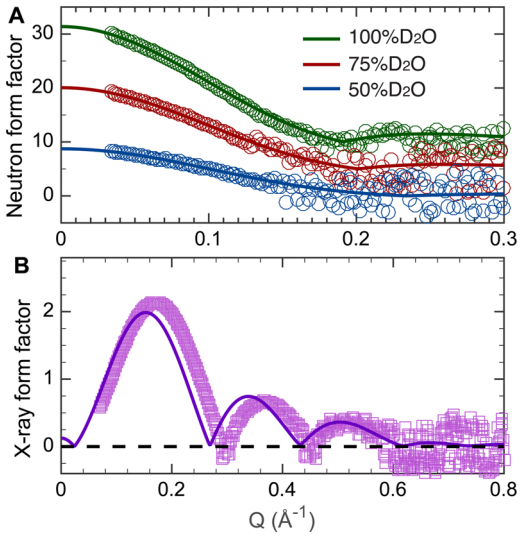

Fig. 3. Model-free comparison between experimental scattering data and a simulated PDPC bilayer with an area per lipid constrained to 72.0 Å^2. The different contrast experimental (A) neutron and (B) X-ray form factors (symbols) are the same as those used in the SDP model analysis. The corresponding simulation form factors (solid lines) were calculated from atom number density distributions obtained from *NAPnT* simulations. Each experimental form factor was scaled by a coefficient to minimize the reduced χ^2, after taking experimental uncertainties into account.

contrast. Both the neutron and the overall χ^2 values are at a minimum for an area per lipid of 72.0 Å^2, whereas the reduced X-ray χ^2 decreases monotonically as the area per lipid increases. Fig. 3 shows the model-free comparison between experimental and simulated form factors for the PDPC bilayer with an area per lipid constrained to 72.0 Å^2. Although the neutron data are in good agreement, this is not the case for the X-ray form factors, especially at the minimum position near 0.3 Å^{-1} a value that relates to the bilayer thickness. Since the minimum position of the simulated X-ray form factor occurs at a smaller q than the experimental X-ray form factor, we can surmise that the simulated bilayer lipid area of 72 Å^2 is too small. This observation partially explains why the X-ray reduced χ^2 becomes smaller when the simulation lipid area increases (and the bilayer thickness decreases). Collectively, Figs. 2 and 3 suggest that the simulated bilayer of A = 72 Å^2 can qualitatively reproduce the experimental scattering data (especially neutron form factors), whereas further tuning of the force field is required to better match the X-ray data and the area per lipid predicted by our SDP model - something that has been noted previously and highlights unresolved issues with simulations (Nagle, 2013). It should be pointed out that the fit to the neutron data leads to A directly (considering only the total molecular volume obtained from densitometry measurements), whereas the X-ray data are sensitive to the values of D_{HH} and D_{H1} from the simulation. Nevertheless, the simulations presented here provide an important basis for the SDP model described below.

3.3. Lateral bilayer area compressibility

Similar to the work of Waheed and Edholm (2009), we used a series of MD simulations to determine the area compressibility modulus from the surface tension at several different lipid areas. Fig. 4 shows the calculated γ of PDPC bilayers at different lipid areas. A linear fit to the data yields an area compressibility modulus of 246.4 mN/m, a value consistent with K_A values of other PC lipids (Rawicz et al., 2000; Braun et al., 2013), and in good agreement with previously determined K_A values for PUFAs (Rawicz et al., 2000).

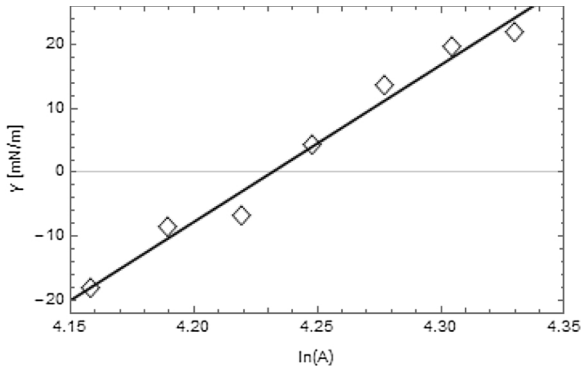

Fig. 4. Lateral surface tension applied to a PDPC bilayer as a function of lipid area (A). The linear fit to the data (solid line) resulted in a calculated area compressibility modulus of K_A = 246.4 mN/m.

3.4. SDP model for PDPC and SDPC

Previous SDP models for phospholipid containing mono-unsaturated fatty chains divided the acyl chains into terminal methyl (CH_3), methine (CH), and methylene (CH_2) groups (Kučerka et al., 2008, 2009, 2011; Pan et al., 2014b). Here, we adopted a similar parsing scheme for PDPC, except for the methine groups. Due to the increased number of olefinic carbons in docosahexaenoyl chains, our modified parsing scheme groups three CH groups into one component, represented by a Gaussian function, as shown in Fig. 5 (CHa and CHb for a total of two components). For the headgroup, we used the same parsing scheme as previous SDP PC models (Kučerka et al., 2008, 2009, 2011), with one exception. Previous SDP analyses of PC lipids used a V_{HL} of 331 Å^3, compared to the 320 Å^3 that we used for the area-constrained PDPC bilayer simulations (A = 72.0 Å^2, please see above). This value for V_{HL} is also consistent with previous experimental headgroup volume measurements (Sun et al., 1994). Importantly, using V_{HL} values of 331 Å^3 and 320 Å^3 results in PUFA areas per lipid that only differ by ~0.5 Å^2, a difference that is considerably smaller than the experimental uncertainty (~1.5 Å^2) that we determined for the final PDPC area.

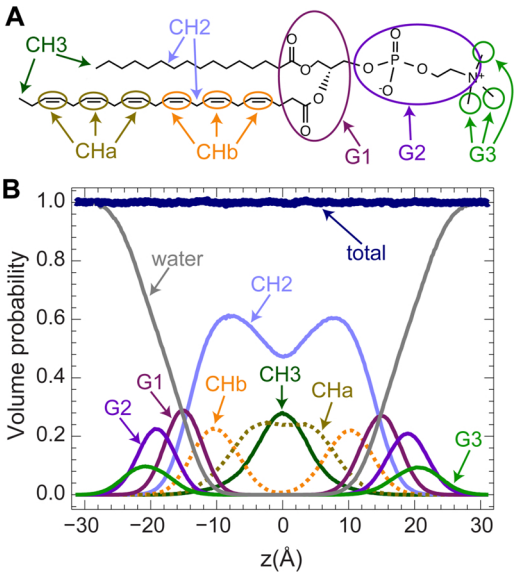

Fig. 5. Parsing scheme for a PDPC bilayer based on MD simulations. (A) The chemical structure of PDPC with different moieties is highlighted. (B) The volume probabilities of each component. Fatty acid chains were divided into terminal methyl (CH_3), methylene (CH_2) and methine (CH), with double bonds grouped together as CHa and CHb. The PC headgroup was parsed into the carbonyl-glycerol (G1), phosphate + CH2CH2N (G2), and choline methyls (G3).

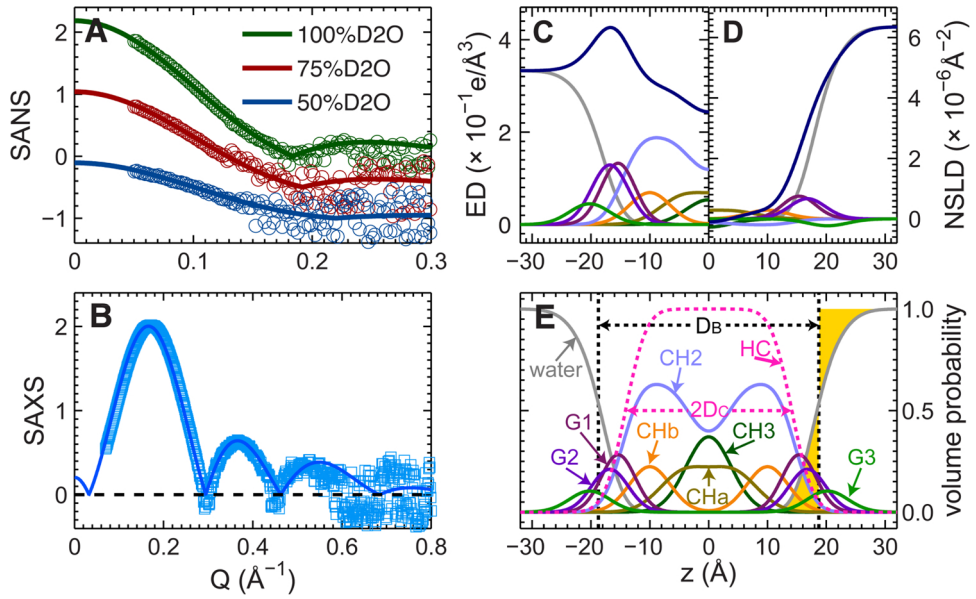

Fig. 6. Fits (solid lines) to the experimental SANS (A) and SAXS (B) form factors (points) for PDPC at 30 °C using SDP. Panels on the right show the SDP model of the PDPC bilayer in real space, where the top panels show electron densities (C) and neutron scattering length densities (D) of the components making up the bilayer, including the total scattering densities (thick lines). (E) Bottom panel illustrates the volume probability distributions, where the total probability is equal to 1 at each point along the bilayer normal.

Similar to our previous SDP model-based analyses (Kučerka et al., 2008, 2011, 2015; Pan et al., 2014a,b), certain parameters were constrained to enhance the robustness of the fits to the data. Specifically, in addition to , the experimentally determined V_L was fixed and soft constraints were applied to a group of parameters, whereby any deviation from the target values determined from MD simulations resulted in a quadratic penalty to the overall χ^2 – soft-constrained parameters are denotated by an asterisk (*). Finally, the distance between two CH components (i.e., $z_{CHb} - z_{CHa}$) was constrained. In the absence of such constraint, the CHs tended to move in opposite directions, resulting in unphysical distances between the two moieties.

3.5. Joint SANS/SAXS analysis

An SDP example used to jointly refine PDPC bilayer SANS and SAXS data at 30 °C is shown in Fig. 6. The volume probability of each component (Fig. 6E) is scaled by the component electron number and neutron scattering length to, respectively, generate ED (Fig. 6C) and NSLD (Fig. 6D) profiles. The X-ray (Fig. 6B) and neutron (Fig. 6A) form factors are the Fourier transform of the total ED and NSLD profiles (after subtracting for bulk water), respectively. Results of these fits are presented in Table 1 for PDPC at 20 °C, 30 °C, and 40 °C, as well as for SDPC at 30 °C. Table 1 also compares structural parameters obtained from the area-constrained MD simulations.

An important parameter commonly used to describe lipid bilayer structures is A, which is determined through a combination of lipid volumetric measurements and the bilayer thickness. Specifically, A is related to the overall bilayer thickness, D_B, through the relationship $A = 2V_L/D_B$, where V_L is the total lipid volume and D_B is the Luzzati bilayer thickness, i.e., the Gibbs dividing surface found between the bilayer and water (Nagle and Tristram-Nagle, 2000). Alternatively, A can be calculated based on the hydrocarbon chain thickness, D_C, which corresponds to the interface between the polar/nonpolar parts, i.e., $A = V_{HC}/D_C$. Other structural parameters listed in Table 1 are the headgroup-to-headgroup distance, D_{HH}, and the distance between the glycerol and phosphate groups, D_{H1}. Finally, σ_{HC} is the width of the error function describing the total hydrocarbon chain region, z_{CHi} and σ_{CHi} are the Gaussian center and width of the components (CHa, CHb, CH3, G1, G2 and G3). r_{CH} and r_{CH3} are the volume ratios of V_{CH}/V_{CH2} and V_{CH3}/V_{CH2}, where V_{CH}, V_{CH2}, and V_{CH3} refer to the average volumes of the CH, CH2 and CH3 components, respectively, and r_{G1} and r_{G2} are the volume fractions, respectively, of the G1 and G2 components with respect to the total headgroup volume.

SDP analysis of PDPC bilayers at 30 °C resulted in an area per lipid of 71.1 Å^2, in good agreement with the 72.0 Å^2 determined by MD simulations (Table 1). This difference is mainly due to the following: (i) D_B, which in conjunction with V_L determines the area per lipid, is more accurately obtained from SANS data; and (ii) the reduced SANS χ^2 value is smallest at 72.0 Å^2 (i.e., the simulation of neutron form factors at 72.0 Å^2 agrees best with the experimental data). The discrepancy between the MD data and the X-ray form factor (Fig. 3) is reflected by the difference in D_{HH} values between the simulated bilayer and the SDP model prediction. The larger D_{HH} value from the simulated bilayer indicates that simulations with smaller D_{HH} will agree better with the experimental X-ray form factor. (Note, that D_{HH} is defined by the maxima in the ED profile.)

Compared to previously reported SDP data for mixed chain lipids, the area per lipid value for PDPC at 30 °C is ~7 Å^2 larger than that of POPC lipids (i.e., 64.3 Å^2) (Kučerka et al., 2011). Consistent with the lipid area result, the hydrocarbon chain thickness, $2D_C$, of PDPC bilayers is ~1 Å smaller than that of POPC bilayers (Kučerka et al., 2011). The values for A and $2D_C$ for PDPC are consistent with a disordered *sn*-2 PUFA chain. Not surprisingly, a monotonically increasing area per lipid with increasing temperature observed for PDPC is consistent with what has been reported previously (Kučerka et al., 2011). Similarly, the area per lipid of SDPC is ~4.9 Å^2 larger than its mono-unsaturated analogue, SOPC (i.e., 65.5 Å^2) (Kučerka et al., 2011), along with its associated invariance of $2D_C$. Interestingly, A for SDPC is identical, within experimental error, to PDPC. That is, exchanging the palmitoyl fatty acid chain with one made from stearoyl does not affect lipid packing, as this bilayer property is dominated by the presence of the disordered docosahexaenoyl acyl chain at the *sn*-2 position. Unfortunately, a direct comparison of PDPC and SDPC with their fully saturated analogues is not possible at these temperatures, as di-palmitoyl PC and di-stearoyl PC only exist in the gel phase at the reported temperatures. The other thickness parameters associated with PDPC and SDPC are notably smaller than their mono-unsaturated analogues; i.e., D_B and D_{HH} are ~2 Å and ~4 Å smaller, respectively. This

Table 1
SDP structural data of PDPC bilayers.

	PDPC				SDPC
	SDP model	SDP model	SDP model	CHARMM	SDP model
	20 °C	30 °C	40 °C	30 °C	30 °C
V_L (Å^3)	1296.6**	1306.4**	1316.1**	1312.0	1366.4**
V_{HL}(Å^3)	320.0**	320.0**	320.0**	320.0	320.0**
A (Å^2)	69.3	71.1	72.9	72.0	70.4
D_B (Å)	37.4	36.8	36.1	36.4	38.8
D_{HH} (Å)	33.2	33.0	32.2	36.8	35.2
$2D_C$ (Å)	28.2	27.8	27.3	27.5	29.7
D_{H1} (Å)	2.51	2.63	2.43	4.63	2.73
z_{G1} (Å)	15.3	14.9	14.6	15.0	16.1
σ_{G1} (Å)	2.84	2.82	2.70	2.88	2.89
z_{G2} (Å)	16.7	17.0	16.6	19.0	17.7
σ_{G2} (Å)	3.23	3.30	3.37	2.95	3.14
z_{G3} (Å)	20.2*	20.0*	19.9*	20.5	20.9*
σG3 (Å)	3.45*	3.44*	3.44*	3.46	3.46*
zCHb (Å)	8.6	8.00	7.8	10.1	8.0
σCHb (Å)	3.52*	3.52*	3.52*	3.50	3.51*
zCHa (Å)	2.8	2.2	2.0	4.3	2.3
σCHa (Å)	4.08*	4.07*	4.07*	4.1	4.08
$z_{CHb} - z_{CHa}$ (Å)	5.8*	5.8*	5.8*	5.8	5.7*
σ_{HC} (Å)	2.84*	2.84*	2.83*	2.83	2.82*
σ_{CH3} (Å)	3.70*	3.70*	3.70*	4.20	3.88*
r_{G1}	0.45*	0.44*	0.44*	0.45	0.45*
r_{G2}	0.36*	0.36*	0.36*	0.36	0.36*
r_{CH3}	2.02*	2.02*	2.02*	1.97	2.01*
r_{CH}	0.92*	0.92*	0.92*	0.92	0.92*

Parameters are shown with their appropriate units for length (Å), area (Å^2), and volume (Å^3). Estimated uncertainties are ±2%. The double asterisk (**) denotes fixed parameters, while a single asterisk (*) denotes "soft" constrained parameters, allowed to vary within certain limits.

observation is consistent with the notion of the PUFA chain "snorkeling" up to the lipid headgroup region. It should be noted that PUFA chains reside at the lipid-water interface an appreciable amount of time, thereby necessitating that the headgroups remain in its tilted orientation in order to shield the PUFAs (umbrella model) (Huang and Feigenson, 1999) from the aqueous solvent, similar to what has previously been seen in POPC and SOPC bilayers (Nagle, 2017). It is worth noting that the dependency of area per lipid on acyl chain length is sensitive to the unsaturation and position of double bonds, mismatch in the unsaturation and length of the two chains, and likely to other structural lipid features (Petrache et al., 2001; Rajamoorthi et al., 2005). For example, the area decrease with increasing chain length was reported for di-saturated PCs, while the elongation of the saturated chain in the case of saturated/mono-unsaturated lipids resulted in area per lipid increase (Harroun et al., 2006).

Subtle, but important differences in lipid bilayer structure induced by the presence of a PUFA chain, rather than a mono-unsaturated chain, can also have profound biological implications. The transverse structure of a membrane has implications associated with integral protein stability, enzyme activation, and modulating charge–membrane interactions (Li et al., 2012). These results are yet another example of the importance of lipid diversity and how different lipid species affect the transmembrane structure.

4. Summary

We combined MD simulations with differently contrasted SANS and SAXS data to determine the structure of the PUFA containing phospholipids, PDPC and SDPC, with a high degree of structural detail. Simulations guided a model-based analysis of the experimental data that resulted in an area per lipid of 71.1 Å^2 for PDPC at 30 °C. This result was supported by a model free analysis of PDPC bilayers, where simulations with different fixed areas per lipid were directly compared to experimental data, yielding an area per PDPC of 72.0 Å^2. Future work will make use of the current SDP model and strategy to determine the bilayer structures for other commonly studied PUFA containing phospholipids. Importantly, the discrepancy between the different contrast scattering and simulations data- considering that the neutron and X-ray data sets were obtained using similarly prepared LUVs- emphasizes the need for the further refinement of the MD simulation force fields.

Conflicts of interest

The authors declare no conflicts of interest.

Acknowledgements

SANS data were collected at the Bio-SANS instrument located at the High Flux Isotope Reactor, a DOE Office of Science User Facility operated by the Oak Ridge National Laboratory. The authors also wish to acknowledge personnel support from the Center for Structural Molecular Biology, funded by the Office of Biological and Environmental Research (BER). J.K. is supported through the Scientific User Facilities Division of the Department of Energy (DOE) Office of Science, sponsored by the Basic Energy Science (BES) Program, DOE Office of Science, under Contract No. DEAC05-00OR22725. F.A.H acknowledges support from National Science Foundation grant No. MCB-1817929. D.M. acknowledges the support of the Natural Sciences and Engineering Research Council of Canada (NSERC), [funding reference number RGPIN-2018-04841].

References

Arnold, O., Bilheux, J., Borreguero, J., Buts, A., Campbell, S., Chapon, L., Doucet, M., Draper, N., Ferraz Leal, R., Gigg, M., Lynch, V., Markvardsen, A., Mikkelson, D., Mikkelson, R., Miller, R., Palmen, K., Parker, P., Passos, G., Perring, T., Peterson, P., Ren, S., Reuter, M., Savici, A., Taylor, J., Taylor, R., Tolchenov, R., Zhou, W., Zikovsky, J., 2014. Mantid-Data analysis and visualization package for neutron scattering and μSR experiments. Nucl. Instrum. Methods Phys. Res. Sect. A: Accel. Spectrom. Detect. Assoc. Equip. 764, 156–166. https://doi.org/10.1016/j.nima.2014.07.029.

Berger, O., Edholm, O., Jähnig, F., 1997. Molecular dynamics simulations of a fluid bilayer of dipalmitoylphosphatidylcholine at full hydration, constant pressure, and

constant temperature. Biophys. J. 72, 2002–2013. https://doi.org/10.1016/S0006-3495(97)78845-3.
Braun, A.R., Sachs, J.N., Nagle, J.F., 2013. Comparing simulations of lipid bilayers to scattering data: the GROMOS 43A1-S3 force field. J. Phys. Chem. B 117, 5065–5072. https://doi.org/10.1021/jp401718K.
Catalá, A., 2012. Lipid peroxidation modifies the picture of membranes from the "Fluid Mosaic Model" to the "Lipid Whisker Model". Biochimie 94, 101–109. https://doi.org/10.1016/j.biochi.2011.09.025.
Darden, T., York, D., Pedersen, L., 1993. Particle mesh Ewald: an N log(N) method for Ewald sums in large systems. J. Chem. Phys. 98, 10089–10092. https://doi.org/10.1063/1.464397.
Eldho, N.V., Feller, S.E., Tristram-Nagle, S., Polozov, I.V., Gawrisch, K., 2003. Polyunsaturated docosahexaenoic vs docosapentaenoic acid. Differences in lipid matrix properties from the loss of one double bond. J. Am. Chem. Soc. 125, 6409–6421. https://doi.org/10.1021/ja029029o.
Feller, S.E., Zhang, Y., Pastor, R.W., Brooks, B.R., 1995. Constant pressure molecular dynamics simulation: the Langevin piston method. J. Chem. Phys. 103, 4613–4621. https://doi.org/10.1063/1.470648.
Feller, S.E., Gawrisch, K., MacKerell, A.D., 2002. Polyunsaturated fatty acids in lipid bilayers: intrinsic and environmental contributions to their unique physical properties. J. Am. Chem. Soc. 124, 318–326. https://doi.org/10.1021/ja0118340.
Gawrisch, K., Eldho, N.V., Holte, L.L., 2003. The structure of DHA in phospholipid membranes. Lipids 38, 445–452. https://doi.org/10.1007/s11745-003-1082-0.
Hamilton, J., Greiner, R., Salem, N., Kim, H.-Y., 2000. n-3 Fatty acid deficiency decreases phosphatidylserine accumulation selectively in neuronal tissues. Lipids 35, 863–869. https://doi.org/10.1007/S11745-000-0595-x.
Harroun, T.A., Katsaras, J., Wassall, S.R., 2006. Cholesterol hydroxyl group is found to reside in the center of a polyunsaturated lipid membrane. Biochemistry 45, 1227–1233. https://doi.org/10.1021/bi0520840.
Harroun, T.A., Katsaras, J., Wassall, S.R., 2008. Cholesterol is found to reside in the center of a polyunsaturated lipid membrane. Biochemistry 47, 7090–7096. https://doi.org/10.1021/bi800123b.
Heberle, F.A., Petruzielo, R.S., Pan, J., Drazba, P., Kučerka, N., Standaert, R.F., Feigenson, G.W., Katsaras, J., 2013. Bilayer thickness mismatch controls domain size in model membranes. J. Am. Chem. Soc. 135, 6853–6859. https://doi.org/10.1021/ja3113615.
Hodzic, A., Rappolt, M., Amenitsch, H., Laggner, P., Pabst, G., 2008. Differential modulation of membrane structure and fluctuations by plant sterols and cholesterol. Biophys. J. 94, 3935–3944. https://doi.org/10.1529/biophysj.107.123224.
Huang, J., Feigenson, G.W., 1999. A microscopic interaction model of maximum solubility of cholesterol in lipid bilayers. Biophys. J. 76, 2142–2157. https://doi.org/10.1016/S0006-3495(99)77369-8.
Jo, S., Lim, J.B., Klauda, J.B., Im, W., 2009. CHARMM-GUI membrane builder for mixed bilayers and its application to yeast membranes. Biophys. J. 97, 50–58. https://doi.org/10.1016/j.bpj.2009.04.013.
Klauda, J.B., Venable, R.M., Freites, J.A., O'Connor, J.W., Tobias, D.J., Mondragon-Ramirez, C., Vorobyov, I., MacKerell, A.D., Pastor, R.W., 2010. Update of the CHARMM all-atom additive force field for lipids: validation on six lipid types. J. Phys. Chem. B 114, 7830–7843. https://doi.org/10.1021/jp101759Q.
Klauda, J.B., Monje, V., Kim, T., Im, W., 2012. Improving the CHARMM force field for polyunsaturated fatty acid chains. J. Phys. Chem. B 116, 9424–9431. https://doi.org/10.1021/jp304056p.
Kratky, O., Leopold, H., Stabinger, H., 1973. The determination of the partial specific volume of proteins by the mechanical oscillator technique. Methods Enzymol. 27, 98–110. https://doi.org/10.1016/s0076-6879(73)27007-6. http://www.ncbi.nlm.nih.gov/pubmed/4797943.
Kučerka, N., Nagle, J.F., Sachs, J.N., Feller, S.E., Pencer, J., Jackson, A., Katsaras, J., 2008. Lipid bilayer structure determined by the simultaneous analysis of neutron and X-ray scattering data. Biophys. J. 95, 2356–2367. https://doi.org/10.1529/biophysj.108.132662.
Kučerka, N., Gallová, J., Uhríková, D., Balgavý, P., Bulacu, M., Marrink, S.-J., Katsaras, J., 2009. Areas of monounsaturated diacylphosphatidylcholines. Biophys. J. 97, 1926–1932. https://doi.org/10.1016/j.bpj.2009.06.050.
Kučerka, N., Katsaras, J., Nagle, J.F., 2010. Comparing membrane simulations to scattering experiments: introducing the SIMtoEXP software. J. Membr. Biol. 235, 43–50. https://doi.org/10.1007/s00232-010-9254-5.
Kučerka, N., Nieh, M.-P., Katsaras, J., 2011. Fluid phase lipid areas and bilayer thicknesses of commonly used phosphatidylcholines as a function of temperature. Biochim. Biophys. Acta (BBA) – Biomembr. 1808, 2761–2771. https://doi.org/10.1016/j.bbamem.2011.07.022.
Kučerka, N., van Oosten, B., Pan, J., Heberle, F.A., Harroun, T.A., Katsaras, J., 2015. Molecular structures of fluid phosphatidylethanolamine bilayers obtained from simulation-to-experiment comparisons and experimental scattering density profiles. J. Phys. Chem. B 119, 1947–1956. https://doi.org/10.1021/jp511159q.
Leng, X., Kinnun, J.J., Marquardt, D., Ghefli, M., Kučerka, N., Katsaras, J., Atkinson, J., Harroun, T.A., Feller, S.E., Wassall, S.R., 2015. α. Biophys. J. 109, 1608–1618. https://doi.org/10.1016/j.bpj.2015.08.032.
Li, L.B., Vorobyov, I., Allen, T.W., 2012. The role of membrane thickness in charged protein-lipid interactions. Biochim. Biophys. Acta (BBA) – Biomembr. 1818, 135–145. https://doi.org/10.1016/j.bbamem.2011.10.026.
Marquardt, D., Williams, J.A., Kučerka, N., Atkinson, J., Wassall, S.R., Katsaras, J., Harroun, T.A., 2013. Tocopherol activity correlates with its location in a membrane: a new perspective on the antioxidant vitamin E. J. Am. Chem. Soc. 135, 7523–7533. https://doi.org/10.1021/ja312665r.
Martyna, G.J., Klein, M.L., Tuckerman, M., 1992. Nosé-Hoover chains: the canonical ensemble via continuous dynamics. J. Chem. Phys. 97, 2635–2643. https://doi.org/10.1063/1.463940.
Nagle, J.F., 2013. Introductory lecture: basic quantities in model biomembranes. Faraday Discuss 161, 11–29. https://doi.org/10.1039/C2FD20121F.
Nagle, J.F., 2017. Experimentally determined tilt and bending moduli of single-component lipid bilayers. Chem. Phys. Lipids 205, 18–24. https://doi.org/10.1016/j.chemphyslip.2017.04.006.
Nagle, J.F., Tristram-Nagle, S., 2000. Structure of lipid bilayers. Biochim. Biophys. Acta (BBA) – Rev. Biomembr. 1469, 159–195. https://doi.org/10.1016/S0304-4157(00)00016-2.
O'Connor, D.L., Hall, R., Adamkin, D., Auestad, N., Castillo, M., Connor, W.E., Connor, S.L., Fitzgerald, K., Groh-Wargo, S., Hartmann, E.E., Jacobs, J., Janowsky, J., Lucas, A., Margeson, D., Mena, P., Neuringer, M., Nesin, M., Singer, L., Stephenson, T., Szabo, J., Zemon, V., 2001. Growth and development in preterm infants fed long-chain polyunsaturated fatty acids: a prospective, randomized controlled trial. Pediatrics 108, 359–371. https://doi.org/10.1542/peds.108.2.359.
Pan, J., Heberle, F.A., Tristram-Nagle, S., Szymanski, M., Koepfinger, M., Katsaras, J., Kučerka, N., 2012. Molecular structures of fluid phase phosphatidylglycerol bilayers as determined by small angle neutron and X-ray scattering. Biochim. Biophys. Acta (BBA) – Biomembr. 1818, 2135–2148. https://doi.org/10.1016/j.bbamem.2012.05.007.
Pan, J., Marquardt, D., Heberle, F.A., Kučerka, N., Katsaras, J., 2014a. Revisiting the bilayer structures of fluid phase phosphatidylglycerol lipids: accounting for exchangeable hydrogens. Biochim. Biophys. Acta (BBA) – Biomembr. 1838, 2966–2969. https://doi.org/10.1016/j.bbamem.2014.08.009.
Pan, J., Cheng, X., Monticelli, L., Heberle, F.A., Kučerka, N., Tieleman, D.P., Katsaras, J., 2014b. The molecular structure of a phosphatidylserine bilayer determined by scattering and molecular dynamics simulations. Soft Matter 10, 3716. https://doi.org/10.1039/c4sm00066h.
Petrache, H.I., Salmon, A., Brown, M.F., 2001. Structural properties of docosahexaenoyl phospholipid bilayers investigated by solid-state 2h NMR spectroscopy. J. Am. Chem. Soc. 123, 12611–12622. https://doi.org/10.1021/ja011745n. pMID: 11741426.
Phillips, J.C., Braun, R., Wang, W., Gumbart, J., Tajkhorshid, E., Villa, E., Chipot, C., Skeel, R.D., Kalé, L., Schulten, K., 2005. Scalable molecular dynamics with NAMD. J. Comput. Chem. 26, 1781–1802. https://doi.org/10.1002/jcc.20289.
Rajamoorthi, K., Petrache, H.I., McIntosh, T.J., Brown, M.F., 2005. Packing and viscoelasticity of polyunsaturated ω-3 and ω-6 lipid bilayers as seen by 2h NMR and X-ray diffraction. J. Am. Chem. Soc. 127, 1576–1588. https://doi.org/10.1021/ja046453b. pMID: 15686391.
Rawicz, W., Olbrich, K., McIntosh, T., Needham, D., Evans, E., 2000. Effect of chain length and unsaturation on elasticity of lipid bilayers. Biophys. J. 79, 328–339. https://doi.org/10.1016/S0006-3495(00)76295-3.
Ryckaert, J.-P., Ciccotti, G., Berendsen, H.J., 1977. Numerical integration of the cartesian equations of motion of a system with constraints: molecular dynamics of n-alkanes. J. Comput. Phys. 23, 327–341. https://doi.org/10.1016/0021-9991(77)90098-5.
Simopoulos, A.P., 1999. Essential fatty acids in health and chronic disease. Am. J. Clin. Nutr. 70, 560s–569s. https://doi.org/10.1093/ajcn/70.3.560s.
Simopoulos, A.P., 2000. Human requirement for N-3 polyunsaturated fatty acids. Poult. Sci. 79, 961–970. https://doi.org/10.1093/ps/79.7.961.
Simopoulos, A.P., 2004. Omega-6/Omega-3 essential fatty acid ratio and chronic diseases. Food Rev. Int. 20, 77–90. https://doi.org/10.1081/FRI-120028831.
Sonne, J., Hansen, F.Y., Peters, G.H., 2005. Methodological problems in pressure profile calculations for lipid bilayers. J. Chem. Phys. 122, 124903. https://doi.org/10.1063/1.1862624.
Soubias, O., Gawrisch, K., 2007. Docosahexaenoyl chains isomerize on the sub-nanosecond time scale. J. Am. Chem. Soc. 129, 6678–6679. https://doi.org/10.1021/ja068856c.
Stillwell, W., Wassall, S.R., 2003. Docosahexaenoic acid: membrane properties of a unique fatty acid. Chem. Phys. Lipids 126, 1–27. https://doi.org/10.1016/S0009-3084(03)00101-4.
Sun, W.-J., Suter, R.M., Knewtson, M.A., Worthington, C.R., Tristram-Nagle, S., Zhang, R., Nagle, J.F., 1994. Order and disorder in fully hydrated unoriented bilayers of gel-phase dipalmitoylphosphatidylcholine. Phys. Rev. E 49, 4665–4676. https://doi.org/10.1103/PhysRevE.49.4665.
Tuckerman, M., Berne, B.J., Martyna, G.J., 1992. Reversible multiple time scale molecular dynamics. J. Chem. Phys. 97, 1990–2001. https://doi.org/10.1063/1.463137.
Waheed, Q., Edholm, O., 2009. Undulation contributions to the area compressibility in lipid bilayer simulations. Biophys. J. 97, 2754–2760. https://doi.org/10.1016/j.bpj.2009.08.048.